High density polyethylene composites containing alumina-toughened zirconia particles: mechanical and tribological behavior

High density polyethylene composites containing alumina-toughened zirconia particles: mechanical and tribological behavior

M. Di Maro[a,b], D. Duraccio[a]*, G. Malucelli[c], M.G. Faga[a]

[a]*Istituto di Scienze e Tecnologie per l'Energia e la Mobilità Sostenibili (STEMS)-UOS di Torino, Consiglio Nazionale delle Ricerche, Strada delle Cacce 73, 10135 Torino, Italy*

[b]*Dipartimento di Scienze Chimiche della Vita e della Sostenibilità, Università degli Studi di Parma, Parco Area delle Scienze, 11/A, 43124 Parma PR, Italy*

[c]*Politecnico di Torino - Dipartimento di Scienza Applicata e Tecnologia, and local INSTM Unit, Viale Teresa Michel 5, 15121 Alessandria - Italy*

*Corresponding author: Donatella Duraccio donatella.duraccio@stems.cnr.it

Abstract

Alumina-toughened Zirconia (ATZ) was used as filler with the purpose to endow High Density Polyethylene (HDPE) with enhanced mechanical and wear properties, hence widening the application field of the polyolefin as biomaterial. Composites with ATZ percentages ranging between 2 and 12wt% were produced by melt extrusion followed by compression molding. A good filler dispersion was obtained for all the materials, despite the presence of few voids and agglomerates was observed at increasing ATZ loadings. The polymer crystallinity was enhanced by filler incorporation, particularly at high~~er~~ percentages. The combination of high crystallinity and, mainly, lack of voids and agglomerates, appeared responsible for the improvement of Young modulus and mechanical strength. The filler positively affected the wear resistance of the composites under lubricated conditions. Indeed, under dry condition, the filler debris formation, arising from the poor interaction with the polymer matrix, resulted in an increase of the wear volume. Conversely, in the presence of water and fetal bovine serum, the layer adsorbed at the surface promoted an easy removal of the filler debris, hence ~~the~~n highlighting the positive effect of ATZ.

1. Introduction

High Density Polyethylene (HDPE) is one of the most used polymers in commodity markets, as it can be transformed by traditional extrusion, blow and injection molding processes. It is very cheap and shows high performance and service life in many applications, including airplane and automobiles interiors and medical devices. Bio-inertia and biocompatibility have awakened the

interest in such a polymer also in the biomedical field as implant for bone analogue replacement [1-4]. After the pioneering work by Bonfield [4], several studies on hydroxyapatite (HA)/HDPE resulted in composites with mechanical properties and wear resistance unsuitable for major load bearing applications (bone replacement) [5,6]. These materials could be envisaged as replacement of minor load bearing applications such as orbital floor reconstruction (cheek bone) and otologic implants (middle ear drum) [7-9]. Other HDPE composites have been studied in the effort of improving the inorganic filler dispersion and interfacial adhesion with the polymer matrix for their applicability as joint/bone replacements. For example, alumina [10] and partially stabilized zirconia (PSZ) [11,12] have been used as partial replacement of hydroxyapatite in the HDPE/HA composites, showing an improvement of mechanical properties (fracture strength and fretting resistance) [10, 12], meanwhile preserving cell viability [11]. Also graphene oxide [13], carbon nanotubes (CNT) [14,15] and CNT with boron nitride nanoplatelets (BN) [16] have been used for successfully increasing mechanical properties and wear resistance.

Alumina toughened zirconia (ATZ) can be considered as a possible reinforcement for HDPE in biomedical applications. As a bulky component, it is one of the most promising material thanks to its excellent mechanical and tribological properties [17], together with biocompatibility and bioactivity [18]. In our previous works, the addition of ATZ (up to 20 wt%) to Ultra High Molecular Weight Polyethylene (UHMWPE) turned out to be a promising way to enhance Young modulus, yield stress and hardness, without compromising the other mechanical parameters [19,20]. In this light, composites at different concentration of ATZ in HDPE were prepared by melt extrusion technique aiming at studying the influence of ATZ loading, distribution and dispersion on the mechanical behavior (dynamic-mechanical analysis, tensile and impact tests). Tribological investigation was also performed at 37°C (body temperature) under dry and lubricated conditions (both water and fetal bovine serum (FBS) as lubricants. Both positive and negative effects of powders on the wear properties of thermoplastic polymers have been reported so far, and there is no general agreement on the related wear mechanisms [10, 14, 15, 21-24]. Nevertheless, hard fillers as alumina,

silica and zirconia nanoparticles have demonstrated to increase the wear performance over their homopolymers [24, 25, 26]; in this context, the use of ATZ may represent a suitable solution also for increasing wear resistance of HDPE.

A systematic study about the effect of the incorporation of ATZ particles into HDPE on the mechanical and tribological behavior of the resulting composites has not been reported yet. ATZ/HDPE composites may represent a new class of materials exhibiting peculiar features, suitable for different applications, specifically devoted to the biomedical sector. Besides, the ease of processability of proposed composites may overcome the difficulties encountered when UHMWPE matrices are considered.

2 Materials and methods

2.1 Materials and composite preparation

HDPE (HOSTALEN GF 4750), with melt flow index of 0.4g/10min (190°C/2.16kg), was supplied by Lyondell – Basel. Alumina Toughened Zirconia (ATZ) (80 wt% 3Y- TZP and 20 wt% alumina. 3Y- TZP consists of 3 mol yttria- stabilized zirconia) was purchased from Tosoh. HDPE/ATZ composites were prepared in a twin screw extruder (DSM xplore Micro 15cc) at 190°C, 5 minutes of mixing, 60 rpm of speed. Before the processing, ATZ was grinded and dried in a vacuum oven at 80°C for 2h. The mixing ratios of HDPE/ATZ (wt/wt) were 100/0, 99/1, 98/2, 97/3, 95/5, 93/7 and 88/12. The extruded materials were compression molded using a Collin P200T press at 210°C and 15 MPa for 2 minutes. A square shaped mold 100 × 100 mm and 0.5 mm thick was used. For wear resistance measurements, samples were compression molded into 12 mm cylindrical specimens at 25 MPa and 180°C for 15 minutes.

2.2 Characterizations

Scanning Electron microscopy (Zeiss Evo 50 XVP with LaB_6 source) was employed for investigating the morphology of the ATZ powder and the ATZ dispersion and distribution within the polymer matrix. In the last case, the samples were fractured in liquid nitrogen and then pinned up to conductive adhesive tapes and gold-metallized.

The crystallinity degree (χ_c) of HDPE/ATZ composites was evaluated from the Wide Angle X-ray powder diffraction patterns (WAXD), obtained by means of a PW3040/60 X'Pert PRO MPD diffractometer from PANalytical, working at 45 kV and 40 mA and using the Bragg–Brentano geometry (Source: High power ceramic tube PW3373/10 LFF with Cu anode). WAXD profiles were acquired using a Ni-filtered Cu Kα radiation ($\lambda = 0.15418$ nm) with a continuous scan of 0.04°/s (scan step size: 0.0167°; Time per step: 53 s) in the range 5-70°. χ_c was calculated as the ratio between the intensity of the polymer crystalline phase diffraction and the total diffraction intensity. The polymer crystalline phase intensity ($I_{c(PE)}$) was determined by subtracting the amorphous phase ($I_{AM(PE)}$) and the ATZ contribution ($I_{c(ATZ)}$) from the total intensity (I_{TOT}) of the diffraction spectrum. The profile of amorphous phase was approximated by using the profile recorded for an ethylene–propylene copolymer that contained 17.5 mol% of propylene and was synthesized by using a metallocene complex biphenyl cyclopentadienyl fluorenyl zirconium activated at 10°C with methylalumoxane (MAO). The ATZ contribution was estimated by performing WAXD analysis on the ATZ powder in the same conditions adopted for collecting the spectra of HDPE composites.

The following equation (1) was used for the calculation of the crystallinity degree:

$$x_c = \frac{I_{c(PE)}}{I_{TOT} - I_{cATZ}} * 100 \qquad (1)$$

where $I_{c(PE)} = I_{TOT} - I_{AM(PE)} - I_{cATZ}$ and $I_{TOT} = I_{AM(PE)} + I_{c(PE)} + I_{cATZ}$

Dynamic-mechanical (DMTA) analyses were performed using a DMA Q800 (TA Instruments) in tensile configuration and in the 25 -100°C range. The heating rate was 3°C/min, the frequency 1 Hz and the oscillation amplitude in strain-controlled mode 0.05%. The storage modulus (*E'*), loss modulus (*E"*) and tanδ curve were obtained as the average of five experiments.

The tensile properties were evaluated using an Instron 5966 tensile tester. The experiments were carried out at room temperature on the compression-molded samples, according to the standard test method ASTM D882; specimens were 0.5 mm thick and 5 mm wide. The elongation and strain at break and at yield were determined with constant deformation rate, then maintaining the v/L_0 ratio

equal to 10 mm/(mm·min); (v = deformation rate and L_0 = initial length of the specimen). The Young modulus E was measured at a constant rate, given from the ratio v/L_0=0.1 mm/(mm·min). The mean values of the mechanical properties were averaged over at least five tests.

The superstructural morphology of composites (useful for the interpretation of mechanical parameters) was observed in thin films prepared between microscope coverslips by melting the composite samples at 210 °C for 3 min and then cooling them at 20°C/min in order to reproduce the same quenching carried out under the press in a Linkam TP-91 hotstage. The samples were placed between crossed polarizers in a Zeiss MC-80 optical microscope equipped with a camera system. To enhance contrast and determine the sign of the spherulites, a λ wave plate was inserted between the polarizers.

The impact behavior of composites was investigated at room temperature by means of a Zwick/Roell charpy impact tester. V-notched specimens with dimensions of 80 mm x 10 mm x 4 mm were prepared in accordance with ISO 179/1 standard. Four specimens were tested for each composition.

Hardness was measured by a Classic Durometer (Sauter model), according to ASTM D2240 standard to get the values on a Shore D scale. Five repetitions were carried out.

Friction measurements were obtained by means of a CSEM High Temperature Tribometer in ball-on-disk configuration. A polished disk sample (R_a ~ 0.2-0.3 μm) was used as rotating material and an alumina ball of 6 mm in diameter with mirror finish surfaces (R_a ~ 0.05 mm) was used as the counterbody material. The tests were conducted at 37°C under 10 N load, radius of 5 mm, and duration of 25.000 cycles, in dry and lubricating conditions. 20 mL of water and calf bovine serum as simulated body fluid (SBF) were used. SBF was purchased from Sigma Aldrich (product F4135, with hemoglobin, ≤20 mg/dL), and diluted with 0.2% sodium azide (NaN_3) to reduce bacterial degradation, and 20 mM EDTA to minimize the precipitation of calcium phosphate. Four specimens of each composition were tested. The contact load of 10 N in combination with alumina counterbody were used with the purpose to reproduce severe wear conditions.

After the wear tests, the topographical features of the wear scar were investigated by SEM. A golden layer of about10 nm was applied on the worn surface prior the analysis.

The mean friction coefficient (COF) is the average value of the friction coefficient at the steady state. The standard deviation was considered as a friction stability parameter [27]. The wear depth and volume loss of the composites after the tribological test were measured by a contact profilometer (Form Talysurf 120), equipped with a 2 μm diamond conical stylus. The wear volume was calculated by integrating the surface area of each 2D profile (extracted from different locations on 3D profile) over distance. The estimated wear volume was normalized to the load to obtain specific wear rates (*k*)

$$k = \frac{V}{SL} \qquad (2)$$

where V (mm^3) is the volume loss, S is the total sliding distance (m) and L is the applied load (N).

Thermogravimetric analyses (TGA) were performed on about 10 mg of material in the range 50 to 800 °C both in nitrogen and air (heating rate: 10 °C/min; gas flow: 25 ml/min), using a TA Discovery thermo balance (TA Instruments) (experimental error: ± 0.5% wt, ±1 °C).

3. Results

Figure 1 shows some typical SEM micrographs from cryogenically fractured surfaces of HDPE/ATZ 98/2, 95/5, 93/7 and 88/12 composites. All the images show finely and rather uniformly dispersed ATZ particles, considering that the size of the primary particles of ATZ is about 30 nm [19]. The agglomerates (usually below the micron size) become more evident at higher ATZ concentrations (i.e. for HDPE/ATZ 93/7 and 88/12 composites, shown as white arrows in Figure 1C and D). ATZ particles appear detached from the matrix, as indicated by

the presence of voids (white arrows in Figure 1E), suggesting a weak filler-polymer interface.

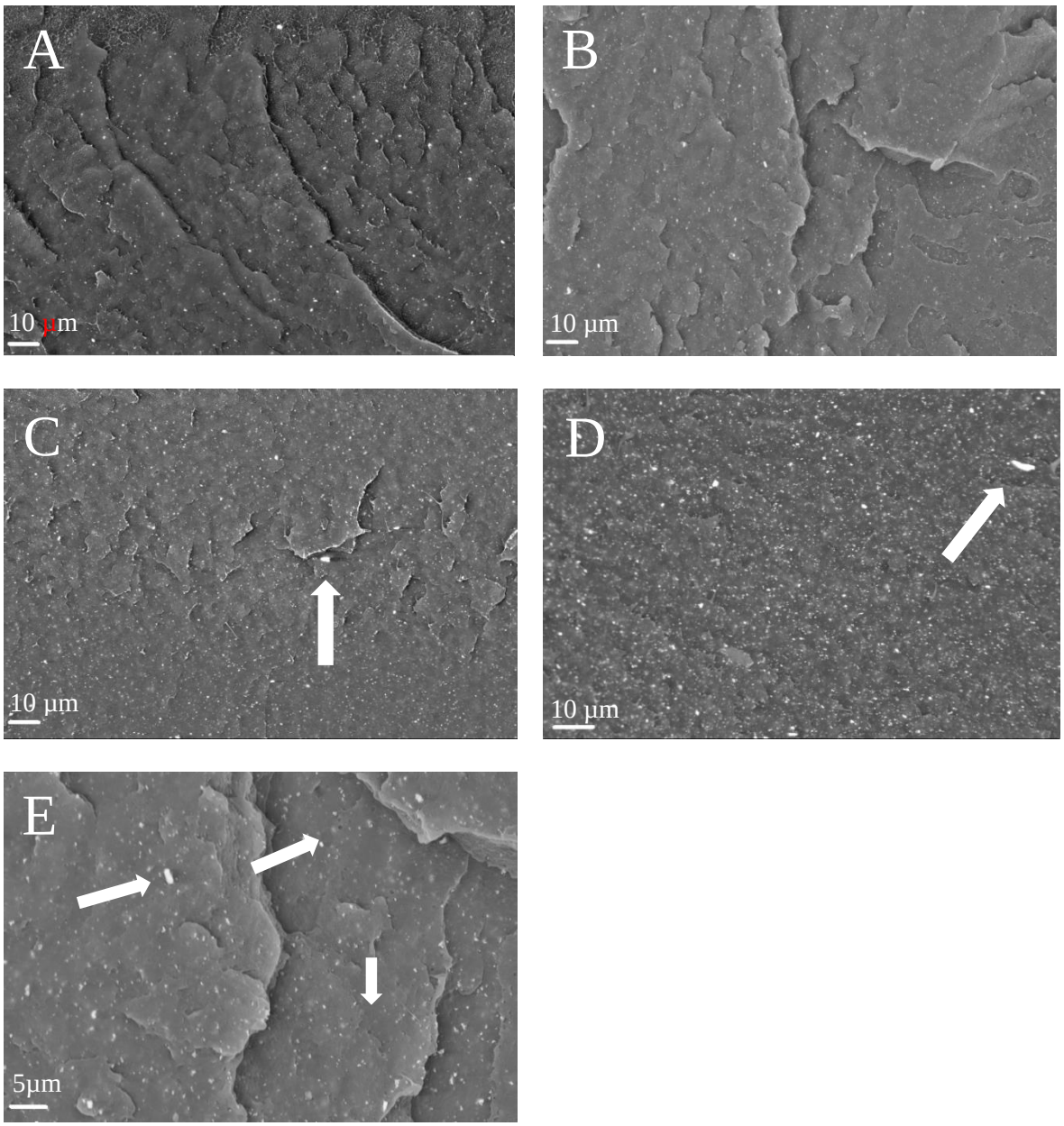

Figure 1. SEM micrographs of fractured surfaces of (A) HDPE/ATZ 98/2; (B) HDPE/ATZ 95/5, (C) HDPE/ATZ 93/7; (D) HDPE/ATZ 88/12 (E) HDPE/ATZ 93/7 at higher magnification.

The WAXD patterns, shown in Figure 2, indicate no significant variation in the crystalline structure of HDPE due to incorporation of ATZ. All the samples crystallize in the orthorhombic form of PE [28], as indicated by the presence of the 110, 200 and 020 reflections at $2\theta = 21°$, 24° and 36°, respectively. The most intense reflections of ATZ at $2\theta = 30$ and 50°, attributable to the 111 and 202 crystallographic planes of the tetragonal) form of ZrO_2 [19], are also visible. The crystallinity values

of the composites (Table 1), are always higher than that of unfilled HDPE, suggesting that ATZ particles act as a heterogeneous nucleating site for crystallization.

Fig. 3A, B and C show the storage modulus (E′), the loss modulus (E″) and tanδ, respectively, as a function of temperature in the range 25 °C - 100 °C. The stiffness of the composites is always slightly higher than that of the unfilled polymer in the whole temperature range (Fig. 3A), proving the reinforcing effect exerted by ATZ. Analogously, the loss modulus (E″) of the composites is higher than that of unfilled HDPE (Fig. 3B). Once again, this finding is an indication of poor interactions occurring between polymer chains and ATZ particles, which causes the presence of microvoids able to dissipate the mechanical stresses. Besides, the α relaxation transition can be noticed in Figure 3B: it appears at 50°C for unfilled HDPE and is due to segmental motion in the amorphous phase in the vicinity of the PE crystalline lamellae [29]. In the composites, the peak intensity of this transition does not decrease, meaning that ATZ particles do not hamper the motion of the amorphous phase. The position of these peaks slightly changes, suggesting that the crystalline superstructure of the matrix is not the same of unfilled HDPE. The poor interfacial interaction and the presence of microvoids are also responsible for the slightly more viscous behaviour of the composites with respect to that of neat HDPE, as indicated by their higher tanδ intensity (Figure 3C).

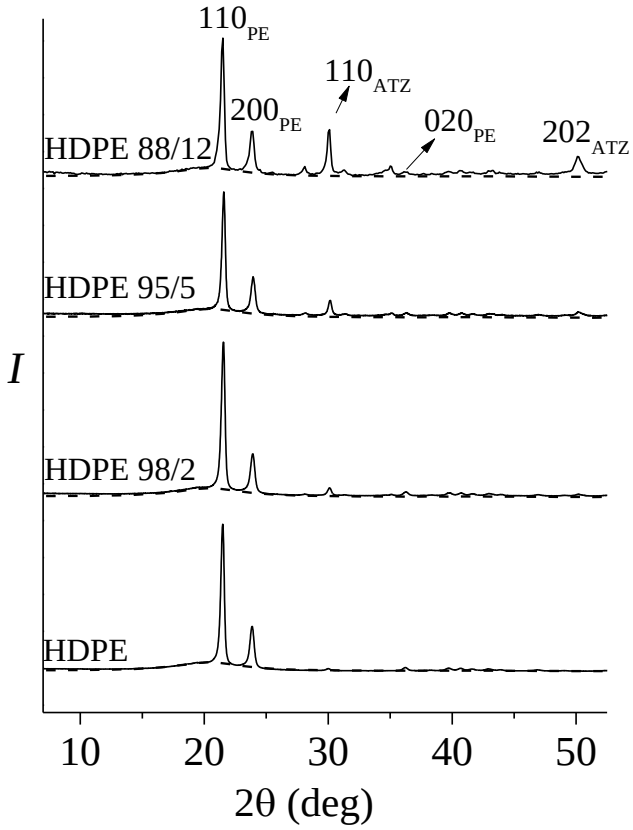

Figure 2. X-ray powder diffraction profiles of HDPE and HDPE/ATZ composites. The contribution from amorphous phase is indicated by the dashed curve. All data have been subtracted from the background intensity approximated as straight line.

The mechanical parameters obtained by stress-strain curves are collected in Table 1. The addition of a few amount of ATZ particles (1-3 wt%) significantly enhances the Young modulus (*E*) of HDPE, reaching an increase of 22% for HDPE/ATZ 99/1, as compared to the unfilled counterpart. A slight increment is also observed for higher ATZ percentages, although the differences among the mean values are limited.

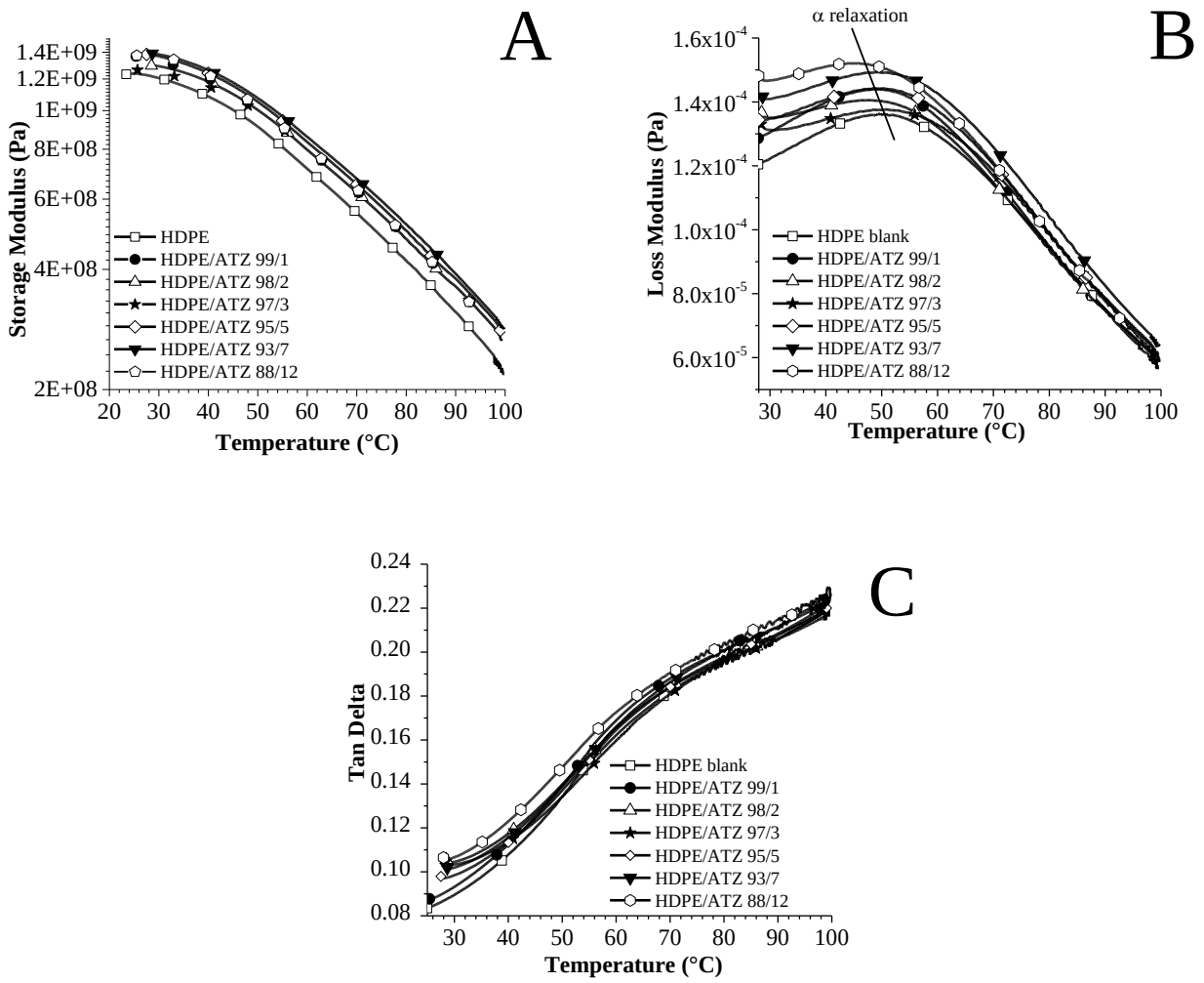

Figure 3. (A) Storage modulus (E'), (B) loss modulus (E") and (C) tanδ of HDPE and its composites.

This behaviour could be explained considering that the crystallinity increase observed for all the composites is hindered by the presence of voids and/or agglomerates, prevailing for ATZ loadings ranging between 5 and 12 wt%. In addition, based on the higher level of crystallinity induced at higher ATZ loadings, it can be supposed that this is not a key parameter for determining the Young modulus enhancement. In a previous work [19], the Young modulus of ATZ/UHMWPE appeared similar for composites with filler percentages ranging between 2.5 and 10 wt%, independently on the crystallinity differences induced on the matrix, supporting the hypothesis of a minor role of this parameter. The actual influence of the presence of agglomerates, is not clearly elucidated in the literature. The agglomeration of filler nanoparticles is also claimed as factor of paramount importance

for enhancing elastic modulus of polymer composites by Dorigato and coworkers, and is not directly related to any change in the crystallinity degree of the polymer matrices [30, 31]. In our case, the presence of ATZ reduces the strength at yield (σ_y) of HDPE by more than 5%, supporting the detrimental effect induced by the presence of aggregates (and voids), hence limiting the potential benefit of the crystallinity increase. The elongation at break (ε_b) is enhanced only when the ATZ is below 5% wt. In literature, the increase in the elongation at break in composites is in general explained through the reduction in the spherulite dimensions and/or by the well-known failure mode characterized by particle debonding: this latter causes the formation of massive voids that coalesce during matrix fibrillation [32, 33].

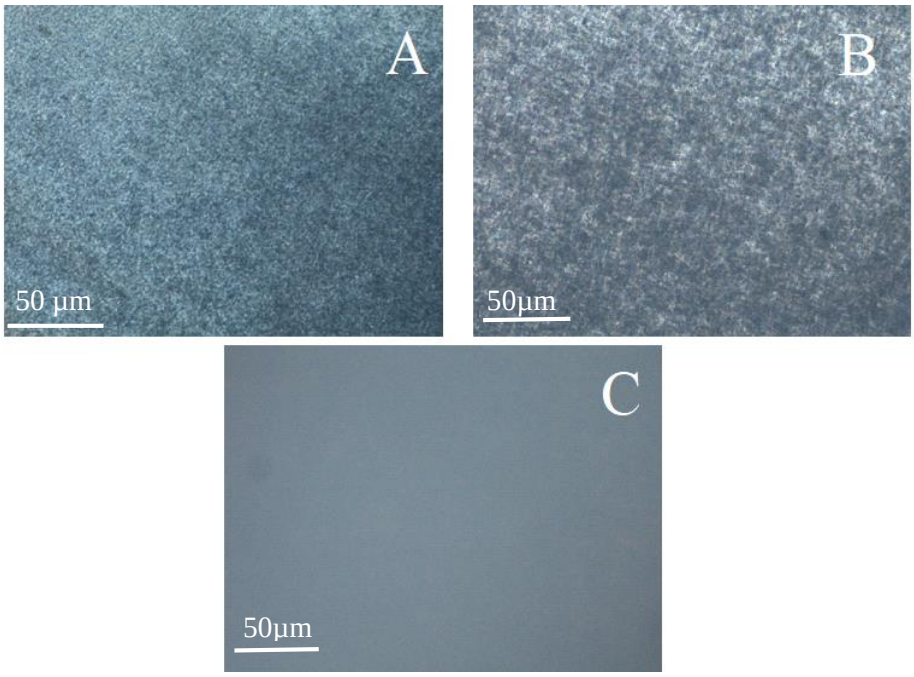

Figure 4. Optical micrographs of thin films prepared between microscope coverslips by melting the composites at 210 °C for 3 min and then cooling at 20°C/min. (A) HDPE, (B) HDPE/ATZ 98/2 and (C) HDPE/ATZ 93/7.

Figure 4 shows the optical images of unfilled HDPE (A), HDPE/ATZ 98/2 (B) and HDPE/ATZ 93/7 (C). The spherulites in HDPE/ATZ 98/2 are similar or slightly bigger than those of HDPE, whereas they decrease significantly at higher ATZ loadings, hence becoming not detectable in HDPE/ATZ 97/3 (Figure C). The change in the spherulites dimensions, often leading to a decrease, supports the hypothesis that ATZ acts as nucleating agent [34]. In addition, higher the ATZ content, higher the

nucleation sites dispersed in the matrix, promoting the formation of larger amount of spherulites. The spherulites growth is hindered by the steric hurdles introduced by well dispersed ATZ particle (few aggregates) that prevent the formation of bigger spherulites crystallites. This well explain the reduction in spherulites dimension evidenced by OM. [35].

The decrease in spherulite size partially agrees with the trend of the elongation at break parameters (Table 1). Indeed, the increase of ε_b can be mainly ascribed to the micro-mechanism failure in polymer composites [32].

Table 1. Crystallinity degree, tensile parameters, impact strength, hardness and "plasticity index" of HDPE and HDPE/ATZ composites.

	HDPE	PE/ATZ 99/1	PE/ATZ 98/2	PE/ATZ 97/3	PE/ATZ 95/5	PE/ATZ 93/7	PE/ATZ 88/12
χ_c (%)	69 ± 2	71 ± 2	73 ± 2	74 ± 2	74 ± 2	75 ± 2	75 ± 2
E (MPa)	969 ± 17	1189 ± 34	1139 ± 16	1125 ± 48	1047 ± 22	1088 ± 53	1001 ± 47
ε_y (%)	8 ± 1	10 ± 1	9 ± 1	8 ± 1	9 ± 1	9 ± 1	8 ± 1
σ_y (MPa)	25 ± 2	24 ± 1	25 ± 1	24 ± 1	24 ± 1	22 ± 1	19 ± 3
ε_b (%)	320 ± 100	647 ± 28	704 ± 85	758 ± 44	270 ± 57	365 ± 145	346 ± 103
σ_b (MPa)	14 ± 1	14 ± 1	15 ± 1	16 ± 1	14 ± 1	12 ± 1	10 ± 2
I_s (kJ/m^2)	10.3 ± 0.5	9.0 ± 0.8	8.6 ± 0.7	9.4 ± 0.4	9.3 ± 0.6	9.2 ± 0.6	9.4 ± 0.9
Shore D	72±1	74±1	73±1	73±2	78±1	77±2	79±3
ShoreD/E	0.074	0.062	0.064	0.065	0.074	0.071	0.072

The Charpy results (Table 1) indicate that the incorporation of ATZ in HDPE leads to a slight decrease of impact strength. It is commonly assumed that inorganic particles, which have weak adhesion to the polymer (as confirmed by SEM images), act as defect, favoring the initiation and propagation of cracks due to a stress concentration effect [36]. This reduction is independent on the ATZ loading.

As expected, Shore D hardness of the composites (Table 1) is always higher than unfilled polymer, due to the intrinsic higher hardness of ATZ with respect to HDPE [19]. The ratio between the Shore D Hardness (H) and the Young modulus (E), also called 'plasticity index", is often used for estimating the wear resistance of the composites [37, 38]. Low H/E values indicate that the work is consumed for the plastic deformation, and the contact material will produce large plastic strain. The calculated plasticity index values of the composites, collected in Table 1, are always lower or similar to that of unfilled HDPE, hence indicating that ATZ worsens the wear resistance of the polymer.

Figure 5 shows the coefficient of friction (COF) as a function of cycles number in dry condition, water and SBF medium for HDPE and HDPE/ATZ 88/12. After the running-in process, the COF

approaches a steady value over all the sliding distances. The steady COF, wear rate and wear depth of HDPE and some composites, representative of low, medium and high ATZ loadings, are summarized in Table 2.

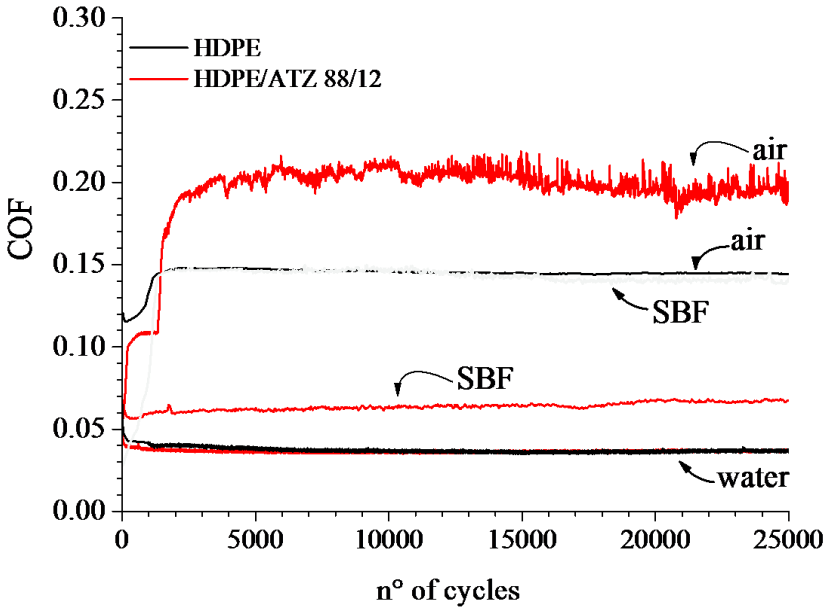

Figure 5. COF as a function of number of cycles in air, water and SBF solution at 37°C for neat HDPE and HDPE/ATZ 88/12. Wear conditions: 25.000 cycles, 10N load, displacement radius of 5mm. Counterbody: 6mm radius alumina ball.

In air, neat HDPE shows a COF value of 0.13 (Table 2). The COF increases with the presence of ATZ, reaching an almost stable value around 0.21, regardeless of ATZ loading. Unfilled HDPE exhibits the lowest wear-resistance (estimated as wear rate and average depth), which is in good agreement with the highest hardness and elastic modulus ratio (Table 1). For the composites, wear rate varies from 2.2×10^{-5} $mm^3/N\cdot m$ (for HDPE/ATZ 98/2 composite) to 5.1×10^{-5} $mm^3/N\cdot m$ (for HDPE/ATZ 88/12 composite), the wear depth from 12.4 to 21.4 μm, respectively.

The tribological behaviour can be interpreted with one of the most accredited wear mechanisms in which, after initial wear cycles, the real tribo-contact is established between polymer surface and a polymeric transfer layer. Such three body wear situation results in a low COF value due to weak-bonding forces (hydrogen bonds and van der Waals forces) among the involved surfaces [39-41].

Table 2. Coefficients of friction and steady-state wear rates for HDPE and its composites in dry condition and when water and bovine serum are used as lubricants.

	HDPE	HDPE/ATZ 98/2	HDPE/ATZ 95/5	HDPE/ATZ 88/12
Dry condition				
COF	0.13±0.01	0.21±0.03	0.22±0.01	0.20±0.02
Wear rate ($\times$ 10-5mm^3/N·m)	1.8	2.2	3.1	5.1
Average depth (μm)	11.5 ± 0.70	12.4 ± 1.1	16.7 ± 0.6	21.4 ± 2.0
Lubricant: water				
COF	0.04±0.01	0.04±0.01	0.04±0.02	0.04±0.01
Wear rate ($\times 10^{-5}$ mm^3/N·m)	1.4	1.3	1.3	1.10
Average depth (μm)	8.1 ± 1.0	8.2 ± 1.1	8.3 ± 1.2	7.0 ± 0.5
Lubricant: SBF				
COF	0.13±0.02	0.11±0.01	0.10±0.02	0.08±0.02
Wear rate ($\times$ 10-5mm^3/N·m)	2.5	2.8	2.3	1.5
Average depth (μm)	12.8± 1.2	14.3± 0.9	11.3± 1.6	9.0± 1.3

In addition, the asperities on alumina ball encounter softer asperities of HDPE, hence deforming the latter. In the composites, two possible phenomena may occur: 1) the transfer layer is continuously abraded by the fine but harder ATZ particles embedded in HDPE; 2) ATZ debris can be incorporated into the transfer film, leading to its strengthening. Both phenomena result in an increase of COF with respect to that of unfilled HDPE. Besides, this severe abrasive wear increases the wear rate and the depth of worn scar. This hypothesis is supported by the increase of wear volume as a function of ATZ loading and by SEM observation. In fact, the worn surfaces of HDPE and HDPE/ATZ 88/12 (Figure 6A and B, respectively), are characterized by plastic deformation, though a more damaged surface appears in the composite, showing a higher formation of wear debris. water, the COF is 0.04 for all materials~~,~~. This behavior may be ascribed to the alumina ball surface that gets hydrated in presence of water. The formation of $Al(OH)_3$ layer transforms the alumina surface in a highly hydrophilic one, lowering the adhesion between polymer or transfer layer and its counterbody. As a result, COF decreases. The wear parameters are also lower than those calculated in dry condition. The presence of water has a lubricating effect leading to reduced shear stresses in the surface, then decreasing the

wear rate. Although the tests were performed at 37°C, the real temperature in the sliding contact may reach higher values causing polymer softening and leading to a decrease of the load-carrying capacity [42]. The presence of water might cool the polymer, hence reducing the frictional heat. In general, water lubrication may increase or decrease the wear rate of polymers, depending on the material combination and the main wear mechanism involved [43, 44]. Our findings are in agreement with those reported for other polymers sliding against alumina [43]. Finally, it is worthwhile to consider that the adsorbed water layer, formed instantaneously and shared off to generate new surface during cycles, should facilitate the removal of debris and reduce abrasion.

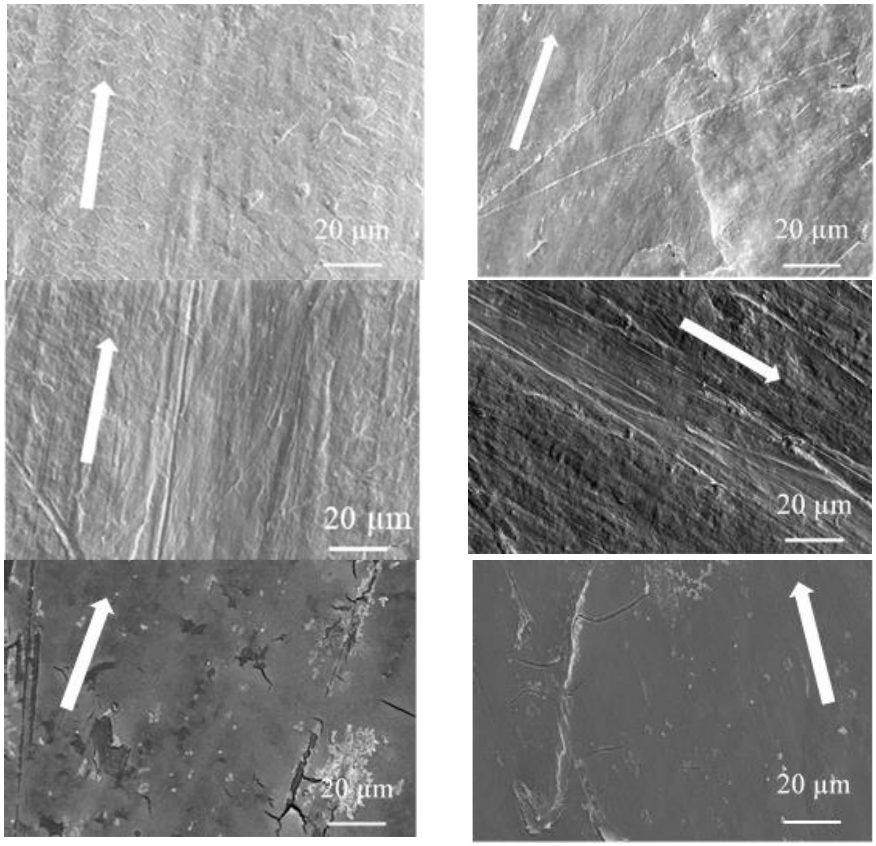

Figure 6. Topographical features of the worn surfaces of HDPE (left) and HDPE/ATZ 88/12 (right) in three different environments: (A) air (B) distillated water and (C) SBF. Arrows indicate the friction direction.

The SEM images displayed in Figure 6C and D, confirm a similar behaviour for HDPE and HDPE/ATZ 88/12: plow grooves with no or limited presence of debris are visible. In SBF, HDPE has almost the same COF (e.g. 0.13) obtained in dry condition, whereas COF of the composites

always decreases. In SBF, COF values are higher than those obtained in water. This could be ascribed to the higher viscosity of SBF with respect to water and to a higher strength of the adsorbed layer by surfaces that require higher shear stress for further sliding [45]. Besides, the frictional heat is not decreased efficiently as in the case of water, possibly causing protein-degradation phenomenon that decreases lubrication ability [43].Interestingly, the wear rates in SBF are higher than those obtained in water and, in some cases, are even higher than those obtained in dry condition, i.e. for HDPE and HDPE/ATZ 98/2 composite. In literature, it is reported that the cited protein-degradation phenomenon can mask the real wear rates [46]. The corroded worn surfaces displayed in Figure 6D and E, which also show the presence of many debris, indicate the possibility of corrosive reactions taking place between polymer surface and complex salts in SBF [10] and also suggest that the involved wear mechanism is particularly complex, with different competing factors that would need much work for being elucidated.

Finally, estimating the plasticity index, can be a reliable method for predicting polymer composites wear only in dry condition. Figure 7 plots TG and dTG curves recorded in N_2 (A) and air (B) for HDPE and some HDPE composites. T_{10} and T_{max} (i.e. the temperatures corresponding to 10% weight loss and to the maximum of the derivative curves, respectively), together with the residue at 700 °C for all the composites, are listed in Table 3.

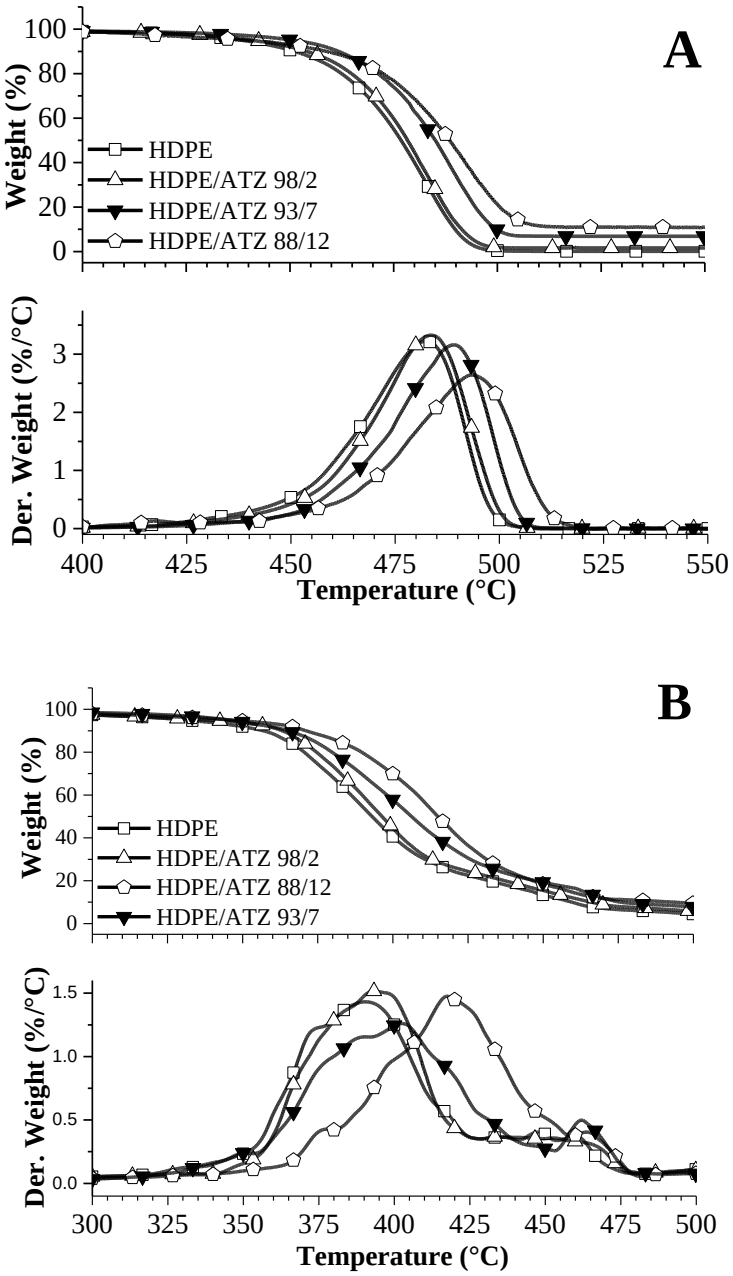

Figure 7. TG and dTG curves of HDPE and some of its composites in nitrogen (A) and air (B).

The thermal and thermo-oxidative stability of HDPE composites is not a fundamental information for materials intended for biomedical applications. However, considering the good mechanical properties of the selected composites, also other applications, in which thermal stability becomes a relevant property, can be taken into account. Besides, thermogravimetric analysis provides information about the real amount of filler dispersed in the polymer matrix (i.e. estimated as the residue at 700°C in air) and suggests an indirect proof of filler dispersion (reproducible curves).

In inert atmosphere, HDPE thermally degrades by a single step centered between 420 and 500°C. In air, a more complex decomposition step is evident and all the pyrolysis products are released as volatile species and no species are converted into a stable residue (that approaches 0 at the end of experiment). HDPE/ATZ composites follow the same behavior of neat HDPE both in inert and in air atmosphere.

However, ATZ influences the thermal degradation process of HDPE: $T_{10\%}$ and T_{max} of the composites are always higher with respect to those of unfilled HDPE. The increase in thermal stability is more pronounced at higher ATZ content (i.e. 95/5, 93/7 and 88/12) and when air is used as testing gas. The highest increase in thermo-oxidative stability can be observed for HDPE/ATZ 88/12: for this system, $T_{10\%}$ and T_{max} are, respectively, 18 and 29 °C higher than those of unfilled HDPE.

The increase in thermal stability is generally attributed first to the filler that can act as a barrier for the degradation of HDPE, slowing the diffusion of the degradation products of the polymer matrix [47, 48]. It may also be ascribed to the higher thermal conductivity of the ceramic material [49] that easily dissipates heat, hence slowing down polymer degradation. The residues at 700°C are in good agreement with the theoretical ATZ content.

Table 3. Thermogravimetric parameters of HDPE/ATZ composites

	N_2			Air		
	T_{10} (°C)	T_{max} (°C)	Residue (@700°C)	T_{10} (°C)	T_{max} (°C)	Residue (@700°C)
HDPE	451	482	0.0	357	390	0
HDPE/ATZ 99/1	452	483	0.8	355	394	0.9
HDPE/ATZ 98/2	453	484	1.6	363	393	1.8
HDPE/ATZ 97/3	458	487	2.7	357	399	2.8
HDPE/ATZ 95/5	461	489	4.8	362	403	4.7
HDPE/ATZ 93/7	462	489	6.9	371	412	6.7
HDPE/ATZ 88/12	463	494	11.4	375	419	11.7

Conclusions

The major outcomes can be summarized as follows:

1) The simple extrusion process allows a good dispersion and distribution of filler in the polymer matrix. The poor interface between polymer and ATZ increases the loss modulus and slightly decreases of the impact strength of the composites.
2) Crystallinity increase and formation of voids and agglomerates seem to play an opposite role in determining the composites stiffness. More specifically, composites with few aggregates and voids (i.e. with low ATZ amount) and limited enhancement of polymer crystallinity lead to an increased polymer stiffness (in terms of both Young and storage moduli). Stiffness decreases at higher ATZ loadings, probably because of the higher amount of aggregates and voids, in spite of a higher crystallinity induced in the matrix. ATZ is also responsible for higher hardness of the composites with respect to unfilled HDPE.
3) ATZ in limited content (1-3wt%) increases the elongation at break (ε_b) because of the recognized micro-mechanism of failure in polymer composites.
4) The wear behavior of HDPE/ATZ composites is significantly affected by the presence and type of lubricant. In dry condition, the effects of the filler on the wear resistance are likely due to the higher surface hardness of the composite and to the contribution of the filler to the transfer film. As result, higher COF and wear rate values are observed in the composites as compared to unfilled HDPE. In water, the effect of the filler is completely annulled; the relevant factors include the decrease of frictional heat, the reduced shear stresses and the debris removal. In SBF medium, some adverse reactions can mask the real wear rates. In this condition, it seems that ATZ exerts a positive effect on the COF decrease.

   In the light of the mechanical and wear results in lubricant conditions, these composites could be promising candidates for moderate load bearing orthopedic applications.

References

[1] N.C. Paxton, M.C. Allenby, P.M. Lewis, M.A Woodruff, Biomedical applications of polyethylene, Eur. Polym. J. 118 (2019) 412–428. https://doi.org/10.1016/j.eurpolymj.2019.05.037.

[2] S. Ramakrishna, J. Mayer, E. Wintermantel, K.W. Leong, Biomedical applications of polymer-composite materials: a review, Compos. Sci. Technol. 61 (2001) 1189–224. https://doi.org/10.1016/S0266-3538(00)00241-4.

[3] K. Sevin, I. Askar, A. Saray, E. Yormuk, Exposure of high-density porous polyethylene (Medpor®) used for contour restoration and treatment, Br. J. Oral. Maxillofac. Surg. 38 (2000) 44–49. https://doi.org/10.1054/bjom.1998.0038.

[4] W. Bonfield, M.D. Grynpas, A.E. Tully, J. Bowman, J. Abram, Hydroxyapatite reinforced polyethylene — a mechanically compatible implant material for bone replacement, Biomaterials 2 (1981) 185-186. https://doi.org/10.1016/0142-9612(81)90050-8.

[5] W. Bonfield, Properties of bone as a material. In: Burny F, Pruers R, editors. Monitoring of orthopaedic implants. Elsevier Science Publishers, Amsterdam; 1993. pp 4–11.

[6] T.S. Keller, Z. Mao, D.M. Spengler, Young's modulus, strength and tissue physical properties of human compact bone, J. Orthop. Res. 8 (1990) 592–603. https://doi.org/10.1002/jor.1100080416.

[7] K.E. Tanner, R.N. Downes, W. Bonefield, Clinical application of hydroxyapatite reinforced polyethylene, Br. Ceram. Trans. 93 (1994) 104–107.

[8] M. Wang, L.L. Hench, W. Bonfield, Bioglass®/high density polyethylene composite for soft tissue applications: preparation and evaluation, J. Biomed. Mater. Res. 42 (1998) 577-586. http://dx.doi.org/10.1002/(SICI)1097-4636(19981215)42:4<577::AID-JBM14>3.0.CO;2-2

[9] R.E. Swain, M. Wang, B. Beale, W. Bonfield, HAPEX (TM) for otologic applications, Biomed Eng: Appl. Basis Commun. 11 (1999) 315-20.

[10] S. Bodhak, S. Nath, B. Basu, Friction and Wear Properties of Novel HDPE—HAp—Al2O3 Biocomposites against Alumina Counterface, J. Biomater. Appl. 23 (2009) 407-433. https://doi.org/10.1177/0885328208090012.

[11] A. Yari Sadi, M.A. Shokrgozar, S.S. Homaeigohar, A.R. Khavandi, Biological evaluation of partially stabilized zirconia added HA/HDPE composites with osteoblast and fibroblast cell lines, J. Mater. Sci. Mater. Med. 19 (2008) 2359-2365. https://doi.org/10.1007/s10856-007-3336-7.

[12] A.Yari Sadi, S.S. Homaeigohar, A.R. Khavandi, J. Javadpour, The effect of partially stabilized zirconia on the mechanical properties of the hydroxyapatite–polyethylene composites, J. Mater. Sci. Mater. Med. 15 (2004) 853-858. https://doi.org/10.1023/B:JMSM.0000036272.28022.3a.

[13] R. Upadhyay, S. Naskar, N. Bhaskar, S. Bose, B. Basu, Modulation of Protein Adsorption and Cell Proliferation on Polyethylene Immobilized Graphene Oxide Reinforced HDPE Bionanocomposites. ACS Appl. Mater. Interfaces 8 (2016) 11954−11968. http://dx.doi.org/10.1021/acsami.6b00946.

[14] S.K. Thakur, A. Sharma, N.K. Batra, Tribological characterization of CNT/HDPE polymer nano-composites, Int. J. Theor. Appl. Res. Mech. Eng., 1 (2012), pp. 32-36.

[15] B.B. Johnson, M.H. Santare, J.E. Novotny, S.G. Advani, Wear behavior of carbon nanotube/high density polyethylene composites, Mech. Mater., 41 (2009), 1108-1115. http://dx.doi.org/10.1016/j.mechmat.2009.04.003.

[16] N. D. Badgayan, S.. Sahu,, S. Samanta, P.S. Rama Sreekanth, Assessment of nanoscopic dynamic mechanical properties and B-C-N triad effect on MWCNT/h-BNNP nanofillers reinforced HDPE hybrid composite using oscillatory nanoindentation: An insight into medical applications, J. Mech. Behav. Biomed. Mat. 80 (2018) 180-188. https://doi.org/10.1016/j.jmbbm.2018.01.027.

[17] C. Piconi, G. Maccauro, Zirconia as a ceramic biomaterial, Biomat. 20 (1999) 1-25. https://doi.org/10.1016/S0142-9612(98)00010-6.

[18] A.H. De Aza, J. Chevalier, G. Fantozzi, M. Schehl, R. Torrecillas, Crack growth resistance of alumina, zirconia and zirconia toughened alumina ceramics for joint prostheses, Biomat. 23 (2002) 937-945. https://doi.org/10.1016/S0142-9612(01)00206-X.

[19] D. Duraccio, V. Strongone, G. Malucelli, F. Auriemma, C. De Rosa, F.D. Mussano, T. Genova, M.G. Faga, The role of alumina-zirconia loading on the mechanical and biological properties of UHMWPE for biomedical applications, Comp. Part B 164 (2019) 800–808. https://doi.org/10.1016/j.compositesb.2019.01.097.

[20] D. Duraccio, V. Strongone, M.G. Faga, F. Auriemma, F. Mussano, T. Genova, G. Malucelli, The role of different dry-mixing techniques on the mechanical and biological behavior of UHMWPE/alumina-zirconia composites for biomedical applications, Europ. Polym. J. 120 (2019) 120; 109274. https://doi.org/10.1016/j.eurpolymj.2019.109274.
[21] N. D. Badgayan, S. Samanta, S. K. Sahu, S.B. V. Siva, K. K. Sadasivuni, D. Sahu, P.S. Rama Sreekanth, Tribological behaviour of 1D and 2D nanofiller based high density poly-ethylene hybrid nanocomposites: A run-in and steady state phase analysis, Wear 376–377, part B (2017) 1379-1390. https://doi.org/10.1016/j.wear.2016.12.037.
[22] J. Pelto, V. Heino, M. Karttunen, I. Rytöluoto, H. Ronkainen, Tribological performance of high density polyethylene (HDPE) composites with low nanofiller loading, Wear 460-461 (2020), 203451. https://doi.org/10.1016/j.wear.2020.203451.
[23] T. Tian Liu, B. Li, B. Lively, A. Eyler, W-H. Zhong, Enhanced wear resistance of high-density polyethylene composites reinforced by organosilane-graphitic nanoplatelets, Wear 309 (2014) 43-51. http://dx.doi.org/10.1016/j.wear.2013.10.013.
[24] D.L. Burris, B. Boesl, G.R. Bourne, W.G. Sawyer, Polymeric nanocomposites for tribological applications, Macromol. Mater. Eng. 292 (2007) 387-402. https://doi.org/10.1002/mame.200600416
[25] R.A. Goyal, A.N. Tiwari, Y.S. Negi, High performance nanocomposites for tribological applications: Preparation and characterization, Mater. Sci. Eng. A 486 (2008) 602-610. https://doi.org/10.1016/j.msea.2007.09.047
[26] M. García, M. de Rooij, L. Winnubst, W.E. van Zyl, H. Verwij, Friction and wear studies on nylon-6/SiO2 nanocomposites, J. Appl. Polym. Sci. 92 (2004) 1855-1862. https://doi.org/10.1002/app.20167.
[27] W. Österle, C. Deutsch, T. Gradt, G. Orts-Gil, T. Schneider, I. Dmitriev**a,** Tribological screening tests for the selection of raw materials for automotive brake pad formulations, Tribol. Int. 73 (2014) 148–55. https://doi.org/10.1016/j.triboint.2014.01.017.
[28] C.W. Bunn, The crystal structure of long-chain normal paraffin hydrocarbons. The “shape” of the >CH2 group ,Trans. Farad. Soc. 35 (1939) 482-491.
[29] R. Popli, M. Glotin, L. Mandelkern, R.S. Benson, Dynamic mechanical studies of α and β relaxations of polyethylenes, J. Polym. Sci. Polym. Phys. Ed. 22 (1984) 407-448. http://dx.doi.org/doi:10.1002/pol.1984.180220306.
[30] A. Dorigato, Y. Dzenis, A. Pegoretti, Nanofiller aggregation as reinforcing mechanism in nanocomposites, Procedia Eng. 10 (2011) 894-899. https://doi.org/10.1016/j.proeng.2011.04.147.
[31] A. Dorigato, A. Pegoretti, Y. Dzenis, Filler aggregation as a reinforcement mechanism in polymer nanocomposites, Mechanics Mater. 61 (2013) 79-90. https://doi.org/10.1016/j.mechmat.2013.02.004
[32] G. H. Michler, H.-H. Kausch-Blecken von Schmeling, The physics and micro-mechanics of nano-voids and nano-particles in polymer combinations, Polym. 54 (2013) 3131-3144. https://doi.org/10.1016/j.polymer.2013.03.035.
[33] V. M. Khumalo, J. Karger-Kocsis R. Thomann, Polyethylene/synthetic boehmite alumina nanocomposites: structure, mechanical, and perforation impact properties, J. Mater. Sci. 46 (2011) 422–428. https://doi.org/10.1007/s10853-010-4882-9.
[34] K. M. Seven, J. M. Cogen, J. F. Gilchrist, Nucleating Agents for High-Density Polyethylene—A Review, Polymer Engineering and Science 56 (2016) 541-554. https://doi.org/10.1002/pen.24278.
[35] Q. Yuan, S. Awate, R.D.K. Misra, Nonisothermal crystallization behavior of polypropylene-clay nanocomposites, Eur. Polym. J. 42 (2006) 1994–2003. https://doi.org/10.1016/j.eurpolymj.2006.03.012.
[36] F. Sahnoune, J. M. Lopez Cuesta, A. Crespy, Improvement of the mechanical properties of an HDPE/PS blend by compatibilization and incorporation of CaCO3, Polym. Engin. Sci. 43 (2003) 647-660. https://doi.org/10.1002/pen.10053.
[37] J. Halling, Surface films in tribology, Tribologia 1 (1982)15-23.
[38] K.-B. Park, K.C. Ludema, Evaluation of the plasticity index as a scuffing criterion, Wear 175 (1994) 123-131. https://doi.org/10.1016/0043-1648(94)90175-9.
[39] S. Bahadur, C. Sunkara, Effect of transfer film structure, composition and bonding on the tribological behavior of polyphenylene sulfide filled with nano particles of TiO_2, ZnO, CuO and SiC, Wear 258 (2005) 1411–1421. https://doi.org/10.1016/j.wear.2004.08.009.
[40] S. Bahadur, The development of transfer layers and their role in polymer tribology, Wear 245 (2000) 92–99. https://doi.org/10.1016/S0043-1648(00)00469-5.
[41] S. Gürgen, Wear performance of UHMWPE based composites including nano-sized fumed silica, Composites Part B: Engineering 173 (2019) 106967. https://doi.org/10.1016/j.compositesb.2019.106967.

[42] C. Allen, A. Bloyce, T. Bell, Sliding wear behaviour of ion implanted ultra high molecular weight polyethylene against a surface modified titanium alloy Ti–6Al–4V, Tribology International 29 (6) (1996) 527–534. https://doi.org/10.1016/0301-679X(95)00116-L.
[43] C. Zhu , O. Jacobs, R. Jaskulka, W. Köller, W. Wu, Effect of counterpart material and water lubrication on the sliding wear performance of crosslinked and non-crosslinked ultra high molecular weight polyethylene, Polym. Test. 23 (2004) 665–673. https://doi.org/10.1016/j.polymertesting.2004.01.009.
[44] M. Wang, M. Chandrasekaran, W. Bonfield, J. Mater. Sci.: Mater. Medic. 13 (2002) 607-611. https://doi.org/10.1023/A:1015139213211.
[45] J.Q. Yao, M.P. Laurent, T.S. Johnson, C.R. Blanchard, R.D. Crowninshield ,The influences of lubricant and material on polymer/CoCr sliding friction, Wear 255 (2003) 780–784. https://doi.org/10.1016/S0043-1648(03)00180-7.
[46] I. C. Clarke, F. W. Chan, A. Essner, V. Gooda, C. Kaddick, R. Lappalainen, M. Laurent, H. McKellop, W. McGarry, D. Schroeder, M. Selenius, M. C. Shen, M. Ueno, A. Wang, J. Yao, Multi-laboratory simulator studies on effects of serum proteins on PTFE cup wear, Wear 250 (2001) 188–198. https://doi.org/10.1016/S0043-1648(01)00656-1.
[47] K. Chrissafis, K.M. Paraskevopoulos, E. Pavlidou, D. Bikiaris, Thermal degradation mechanism of HDPE nanocomposites containing fumed silica nanoparticles, Thermochim. Acta 485 (2009) 65-71. https://doi.org/10.1016/j.tca.2008.12.011.
[48] S. Sinha Ray, M. Bousmina, Biodegradable polymers and their layered silicate nanocomposites: in greening the 21st century materials world, Prog. Mater. Sci. 50 (2005) 962-1079. https://doi.org/10.1016/j.pmatsci.2005.05.002.
[49] K. W. Schlichting, N. P. Padture, P. G. Klemens, Thermal conductivity of dense and porous yttria-stabilized zirconia, J. Mat. Sci. 36 (2001) 3003 – 3010. https://doi.org/10.1023/A:1017970924312.